Proceedings of the 12th International Conference on
Computational Fluid Dynamics in the Oil & Gas,
Metallurgical and Process Industries

Progress in Applied CFD – CFD2017

SINTEF

SINTEF Proceedings

Editors:
Jan Erik Olsen and Stein Tore Johansen

Progress in Applied CFD – CFD2017

Proceedings of the 12th International Conference on Computational Fluid Dynamics
in the Oil & Gas, Metallurgical and Process Industries

SINTEF Academic Press

SINTEF Proceedings
SINTEF Proceedings is a serial publication for peer-reviewed conference proceedings
on a variety of scientific topics.
The processes of peer-reviewing of papers published in SINTEF Proceedings are
administered by the conference organizers and proceedings editors. Detailed
procedures will vary according to custom and practice in each scientific community.

PREFACE

This book contains all manuscripts approved by the reviewers and the organizing committee of the 12th International Conference on Computational Fluid Dynamics in the Oil & Gas, Metallurgical and Process Industries. The conference was hosted by SINTEF in Trondheim in May/June 2017 and is also known as CFD2017 for short. The conference series was initiated by CSIRO and Phil Schwarz in 1997. So far the conference has been alternating between CSIRO in Melbourne and SINTEF in Trondheim. The conferences focuses on the application of CFD in the oil and gas industries, metal production, mineral processing, power generation, chemicals and other process industries. In addition pragmatic modelling concepts and bio-mechanical applications have become an important part of the conference. The papers in this book demonstrate the current progress in applied CFD.

The conference papers undergo a review process involving two experts. Only papers accepted by the reviewers are included in the proceedings. 108 contributions were presented at the conference together with six keynote presentations. A majority of these contributions are presented by their manuscript in this collection (a few were granted to present without an accompanying manuscript).

The organizing committee would like to thank everyone who has helped with review of manuscripts, all those who helped to promote the conference and all authors who have submitted scientific contributions. We are also grateful for the support from the conference sponsors: ANSYS, SFI Metal Production and NanoSim.

<div align="right">Stein Tore Johansen & Jan Erik Olsen</div>

Organizing committee:

Conference chairman: Prof. Stein Tore Johansen
Conference coordinator: Dr. Jan Erik Olsen
Dr. Bernhard Müller
Dr.Sigrid Karstad Dahl
Dr.Shahriar Amini
Dr.Ernst Meese
Dr.Josip Zoric
Dr.Jannike Solsvik
Dr.Peter Witt

Scientific committee:

Stein Tore Johansen, SINTEF/NTNU
Bernhard Müller, NTNU
Phil Schwarz, CSIRO
Akio Tomiyama, Kobe University
Hans Kuipers, Eindhoven University of Technology
Jinghai Li, Chinese Academy of Science
Markus Braun, Ansys
Simon Lo, CD-adapco
Patrick Segers, Universiteit Gent
Jiyuan Tu, RMIT
Jos Derksen, University of Aberdeen
Dmitry Eskin, Schlumberger-Doll Research
Pär Jönsson, KTH
Stefan Pirker, Johannes Kepler University
Josip Zoric, SINTEF

CONTENTS

12th International Conference on CFD in Oil & Gas, Metallurgical and Process Industries
SINTEF, Trondheim, NORWAY
May 30th - June 1st, 2017

CFD 2017

IMPLEMENTATION, DEMONSTRATION AND VALIDATION OF A USER-DEFINED WALL FUNCTION FOR DIRECT PRECIPITATION FOULING IN ANSYS FLUENT

Sverre G. JOHNSEN[1][*], **Tiina M. PÄÄKKÖNEN**[2], **Stein T. JOHANSEN**[1][3], **Riitta L. KEISKI**[2], **Bernd WITTGENS**[1]

[1]SINTEF Materials and Chemistry, NO-7465 Trondheim, NORWAY

[2]University of Oulu, Environmental and Chemical Engineering, FI-90014 Oulu, FINLAND

[3]NTNU, Dept. of Energy and Process Engineering, NO-7491 Trondheim, NORWAY

[*] E-mail: sverre.g.johnsen@sintef.no

ABSTRACT

In a previous paper (Johnsen *et al.*, 2015) and presentation (Johnsen *et al.*, 2016), we developed and demonstrated a generic modelling framework for the modelling of direct precipitation fouling from multi-component fluid mixtures that become super-saturated at the wall. The modelling concept involves the 1-dimensional transport of the fluid species through the turbulent boundary layer close to the wall. The governing equations include the Reynolds-averaged (RANS) advection-diffusion equations for each fluid species, and the axial momentum and energy equations for the fluid mixture. The driving force for the diffusive transport is the local gradient in the species' chemical potential. Adsorption mechanisms are not modelled per se, but the time-scale of adsorption is reflected in the choice of Dirichlet boundary conditions for the depositing species, at the fluid-solid interface.

In this paper, the modelling framework is implemented as a user-defined function (UDF) for the CFD software ANSYS Fluent, to act as a wall boundary condition for mass-transfer to the wall. The subgrid, 1-dimensional formulation of the model reduces the computational cost associated with resolving the fine length-scales at which the boundary-layer mass transfer is determined, and allows for efficient modelling of industry-scale heat exchangers suffering from fouling.

The current paper describes the modelling framework, and demonstrates and validates its applicability in a simplified 2D heat exchanger geometry (experimental and detailed CFD modelling data by Pääkkönen *et al.* (2012, 2016)). By tuning the diffusivity, only, good agreement with the experimental data and the detailed CFD model was obtained, in terms of area-averaged deposition rates.

Keywords: CFD, Heat Exchangers, Mass transfer, Multiscale, UDF, Wall function, Fouling .

NOMENCLATURE

Greek Symbols

$\partial_{y^+} \equiv \partial/\partial y^+$ Dimensionless derivative in the wall-normal direction, $[-]$.

$\kappa = 0.42$ von Kármán constant, $[-]$.

μ Dynamic viscosity, $[\text{Pas}]$.

ρ_f Fluid mixture mass density, $[\text{kg/m}^3]$.

τ_w Wall shear stress, $[\text{Pa}]$.

Latin Symbols

c_P Specific heat capacity, $[\text{J/kgK}]$.

C Concentration, $[\text{kg/m}^3]$.

E_a Activation energy, $[\text{J/mol}]$.

$\boldsymbol{g}$ Gravity vector, $[\text{m/s}^2]$.

h_{sens} Specific sensible enthalpy, $[\text{J/kg}]$.

j_{dep} Deposition rate, $[\text{kg/m}^2\text{s}]$.

$\boldsymbol{j}$ Mass flux vector, $[\text{kg/m}^2\text{s}]$.

k_0 Pre-exponential factor, $[\text{m}^4/\text{kgs}^2]$.

k_r' Surface integration rate constant, $[\text{m}^4/\text{kgs}^2]$.

k Thermal conductivity, $[\text{W/mK}]$.

N Number of species, $[-]$.

P Pressure, $[\text{Pa}]$.

Pr Prandtl number, $[-]$.

q_w Wall heat flux, $[\text{W/m}^2]$.

$\mathcal{R}$ Universal gas constant, $[8.3144598 \text{J/Kmol}]$.

Sc Schmidt number, $[-]$.

T Absolute temperature, $[\text{K}[$.

$u_\tau \equiv \sqrt{\tau_w/\rho_{f,w}}$ Shear velocity, $[\text{m/s}]$.

$u_{f,x}$ Fluid velocity parallel to the wall, $[\text{m/s}]$.

$\boldsymbol{u}_f$ Mass-averaged advective fluid velocity vector, $[\text{m/s}]$.

x Cartesian coordinate, parallel to the wall, $[\text{m}]$.

X Mass fraction, $[\text{kg/kg}]$.

y Cartesian coordinate, normal to the wall, $[\text{m}]$.

z Mole fraction, $[\text{mol/mol}]$.

Sub/superscripts

$+$ Dimensionless variable.

a, b, c Curve-fit parameters.

bulk   Value in the bulk.

d Diffusive.

f Property of the fluid mixture.

i Species index.

I Solid-fluid interface.

in   Value at inlet.

reg   Regression value.

Sat   Saturation value.

t Turbulent.

w Value at the wall.

INTRODUCTION

Fouling of solid surfaces and heat exchanger surfaces in particular, is a common and much studied problem in most process industries, as reflected in the review paper by Müller-Steinhagen (2011). Fouling is defined as the unwanted accumulation of solid (or semi-solid) material on solid surfaces. A similar phenomenon is the desired accumulation of solids e.g. in chemical vapor deposition (Krishnan *et al.*, 1994; Kleijn *et al.*, 1989). A common and costly problem in many industrial applications is the direct precipitation of super saturated fluids on heat exchanger surfaces. Typical examples

S. G. Johnsen, T. M. Pääkkönen, S. T. Johansen, R. L. Keiski, B. Wittgens

are found in e.g. the high-temperature off-gas from waste incineration, metal production, or in power plants, where efficient heat recovery is key to sustainable production, and where a combination of direct precipitation and deposition of e.g. solid metal oxides is a major showstopper. Similar issues can be found in almost all process industries, and in the current work we study the deposition of a low-solubility salt (calcium carbonate, $CaCO_3$) from liquid water. By precipitation, we understand all types of phase transitions from a fluid to a relatively denser phase, e.g. gas $\rightarrow$ liquid (condensation), gas $\rightarrow$ solid (sublimation), liquid $\rightarrow$ solid (solidification). For some materials, the precipitate may have a crystalline structure (crystallization)(e.g. $CaCO_3$).

In our modelling work, fouling due to mass deposition from a fluid phase is grouped into two different classes; 1) particulate fouling, where particles carried by the fluid phase penetrate through the laminar boundary layer and stick to the wall (e.g. precipitates, dust, or soot particles) (Johansen, 1991; Johnsen and Johansen, 2009); and 2) direct precipitation where the fluid is super-saturated close to the wall and a phase-transition occurs at the wall (current paper). The direct precipitation on solid surfaces is due to the molecular diffusion through the stagnant boundary layer close to the wall. This is a complex physical process where the diffusion flux of each species is coupled to the diffusion fluxes and thermodynamic/chemical properties of all the species present. Commonly, a combination of 1 and 2 takes place. Fouling can only occur if the adhesive forces between the foulant and the wall are strong enough to overcome the flow-induced shear forces at the wall.

In previous papers, we developed frameworks for the mathematical modelling of particle deposition and re-entrainment (Johansen, 1991; Johnsen and Johansen, 2009) and direct precipitation (Johnsen *et al.*, 2015). In presentations (Johnsen *et al.*, 2010, 2016), it was demonstrated how these models could be employed as wall boundary conditions (mass sinks) for CFD models. Pääkkönen *et al.* (2016) compared CFD simulations with experimental results with respect to $CaCO_3$ deposition in a lab-scale heat exchanger setup. In the current paper we apply the wall function approach published in (Johnsen *et al.*, 2015), in a coarse grid CFD model, and test it against the detailed CFD modelling results and experimental data obtained by Pääkkönen *et al.* (2012, 2016).

EXPERIMENTAL SETUP

The modelling results are validated against experimental data from crystallization fouling on a heated surface. The experimental setup includes a flow-loop with a test-section (a rectangular flow channel), with ohmically heated test surfaces. In the present work, we investigate the case where the wall heat flux was a constant $q_w = 52.5 kW/m^2$. A water-based test liquid, supersaturated with respect to $CaCO_3$, is circulated from a mixing tank and is filtered before entering the test section (average inlet velocities ranging from $u_{f,x,in} = 0.2 - 0.4 m/s$ and temperature of $T_{in} = 303K$), where $CaCO_3$ precipitates and deposits on the heated test surface. The growth of the fouling layer is monitored by measuring the temperature at the test surface. The decreased overall heat transfer coefficient due to the fouling layer (fouling resistance) will cause the test-section surface temperature to increase. Details of the experimental setup, procedure and results were described by Pääkkönen *et al.* (2012).
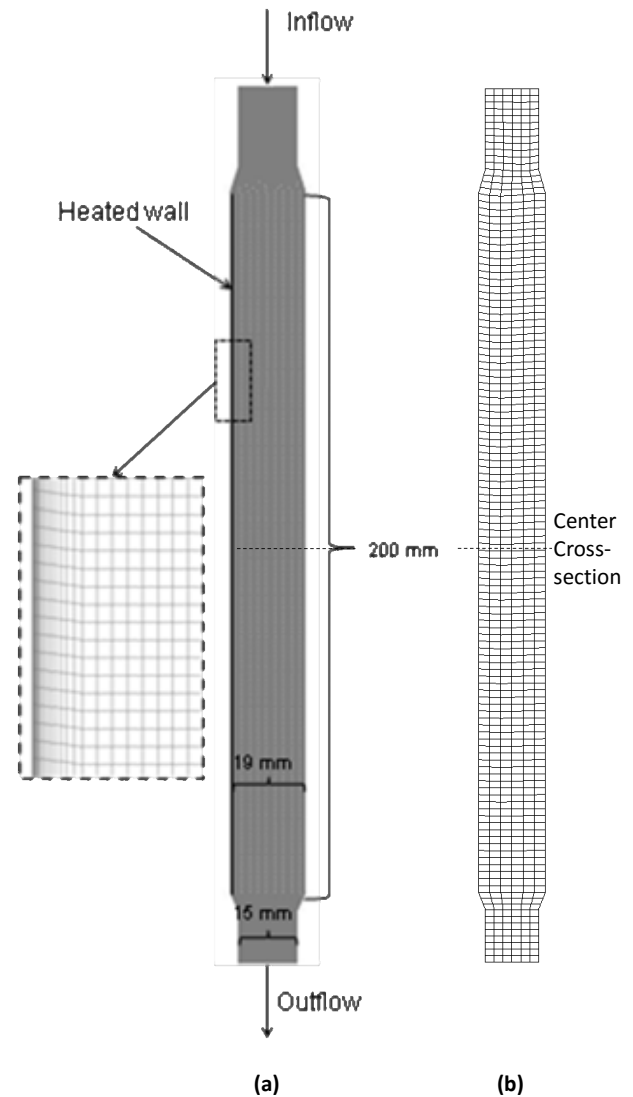
Figure 1: Computational geometry and fine-mesh (a), for two-step fouling model (Pääkkönen *et al.*, 2016), and coarse mesh (b), for fouling wall function model.

MODEL DESCRIPTION

In the present paper, CFD is used to model experiments performed in the aforementioned experimental setup. Two different modelling approaches are employed; 1) *Two-step fouling model* (Pääkkönen *et al.*, 2016); and 2) *Fouling wall function* for direct precipitation fouling (Johnsen *et al.*, 2015, 2016). These two differ fundamentally in the way they approach the problem. Model 1 relies on a detailed CFD mesh close to the wall in order to be able to model the boundary layer phenomena correctly, and employs the traditional two-step approach (see e.g. (Mullin, 2001)) to model the deposition rate. Model 2, on the other hand, relies on a relatively coarse mesh, where the cell centers of the cells residing at the wall are in the log-layer. This approach employs a subgrid model to calculate the deposition rates from a set of simplified governing equations. For more details, see descriptions below as well as mentioned references. The main objective of the current paper is to shed light on the applicability of the wall function approach, since the successful application of such a method would be an essential step towards the cost-efficient modelling of many industry scale applications.

Geometry and Computational Mesh

Figure 1 presents the 2D geometry used in the CFD simulations. The figure shows a 2D-representation of the liquid-filled gap between two parallel, vertical heat transfer surfaces. The liquid enters from the top and exits through the bottom. For more details about the experimental set-up, refer to Pääkkönen *et al.* (2012).

Two different meshes were applied for the two different modelling approaches described below; namely a fine mesh, as shown in Figure 1a (Pääkkönen *et al.*, 2016), and a coarse mesh as shown in Figure 1b. The coarse mesh was used with the wall function model (Johnsen *et al.*, 2015) whereas the fine mesh was used with the two-step model (Pääkkönen *et al.*, 2016). With the fine mesh, the y^+ value at the surface is about 0.08, and the total number of cells is 76000. In the coarse mesh, the y^+ value at the wall is between 20 (for the $u_{f,x,in} = 0.2 m/s$ case) and 36 (for the $u_{f,x,in} = 0.4 m/s$ case), and the total number of cells is 276. In addition, the wall function utilizes a 1-dimensional, logarithmic subgrid consisting of 300 computational nodes, the first node at a wall-distance equal to $1/10000$th of the distance to the cell center in the coarse CFD mesh ($\sim 2.34 \cdot 10^{-7} m$).

Model Fluid

The test liquid in the experiments was a mixture of various salts dissolved in water. Refer to (Pääkkönen *et al.*, 2015) for details. In the current modelling work it was assumed that the test fluid was a pure calcium carbonate, $CaCO_3$, solution in water. Thus, the mixture was considered as a dilute, electrically quasi-neutral ideal mixture with no chemical reactions. In the present paper, the $CaCO_3$ mass-fraction of $4.197 \cdot 10^{-4} kg/kg$ was used for the test fluid entering the model geometry. Temperature-dependent fluid properties (mass density, viscosity, diffusivity) were modelled in accordance with Table 2 in (Pääkkönen *et al.*, 2015).

Fouling Models

Traditionally mass deposition at the wall surface, in crystallization fouling, is modelled based on a two-step approach. In the two-step modelling approach, the fouling process consists of 1) transport from the bulk to the vicinity of the wall, and 2) surface integration (i.e. adsorption onto the fouling layer). The species transport to the vicinity of the crystal-fluid interface, is based on the difference between the bulk and interface concentrations. The mass transfer coefficient is typically estimated from empirical correlations. At the surface, the integration of the species into the crystal body is modelled as a pseudo chemical reaction driven by the difference between the interface and saturation concentrations. When the two steps are combined, the interfacial concentration, which is often unknown, cancels out of the model. The two-step approach has been used as a stand-alone model (Bansal *et al.*, 2008; Helalizadeha *et al.*, 2005; Augustin and Bohnet, 1995) as well as part of a CFD model (Mwaba *et al.*, 2006; Brahim *et al.*, 2003).

Two-step fouling model

Pääkkönen *et al.* (2016) implemented the two-step model into CFD by utilizing the ability of CFD to model the transport of species to the vicinity of the surface, and thus provide the interfacial concentration difference between the surface and the fluid. To account for the wall shear-stress dependency of the adhesion probability seen in experiments (Pääkkönen *et al.*, 2015), a time scaling factor was included in the model to scale the fluid residence time at the wall.

The mass deposition rate to the surface, based on the two-step approach, including the effect of the residence time (Pääkkönen *et al.*, 2015) can be expressed as

$$j_{dep} = \beta \left[\frac{1}{2} \left(\frac{\beta \rho_f u_\tau^2}{k_r' \mu_f} \right) + (C_b - C_{Sat}) - \right.$$
$$\left. - \sqrt{ \frac{1}{4} \left(\frac{\beta \rho_f u_\tau^2}{k_r' \mu_f} \right)^2 + \frac{\beta \rho_f u_\tau^2}{k_r' \mu_f} (C_b - C_{Sat}) } \right] . \quad (1)$$

From the experiments, it was determined that the fouling process was controlled by surface integration (Pääkkönen *et al.*, 2012). Thus, Eq. (1) reduces to

$$j_{dep} = k_r' (C_b - C_{Sat})^2 \frac{\mu_f}{\rho_f u_\tau^2} , \quad (2)$$

where the rate constant for the surface integration can be determined from

$$k_r' = k_0 \exp \left(-E_a / \mathcal{R} T \right) . \quad (3)$$

The pre-exponential factor $k_0 = 1.62 \cdot 10^{22} m^4/kgs^2$, and the activation energy $E_a = 148 kJ/mol$ were determined from the experiments, for the surface integration controlled fouling process (Pääkkönen *et al.*, 2015). The two-step fouling model was implemented into CFD as mass and momentum sink terms.

Fouling wall function

The core idea of the fouling wall function approach is to formulate the species transport equations on one-dimensional form by applying appropriate approximations and simplifications in the turbulent boundary layer. Next, the simplified governing equations are solved on a local subgrid for each grid cell residing at the wall, to obtain the cell-specific deposition mass flux. Thus, the calculated species mass fluxes, at the wall, can be used as mass sinks in the CFD grid cells next to the wall.

The set of steady-state governing equations consists of the Advection-Diffusion equation (ADE) for each species,

$$\nabla \cdot (\rho_f X_i \boldsymbol{u}_f) + \nabla \cdot \boldsymbol{j}_{d,i} = 0 , \quad (4)$$

the fluid mixture momentum and energy equations,

$$\nabla \cdot (\rho_f \boldsymbol{u}_f \boldsymbol{u}_f) = -\nabla P + \nabla \boldsymbol{\tau} + \rho_f \boldsymbol{g} , \quad (5)$$

$$\nabla \cdot (\rho_f h_{sens,f} \boldsymbol{u}_f) = \nabla (k_f \nabla T) - \nabla \left(\sum_i \boldsymbol{j}_{i,d} h_{sens,i} \right) , \quad (6)$$

and the restriction that the mass- and mole-fractions must sum to unity,

$$\sum_i X_i = \sum_i z_i = 1 . \quad (7)$$

Introducing turbulence, dimensionless variables and appropriate simplifications, the simplified governing equations are obtained:

$$\partial_{y^+} \left[\frac{\nu_t^+}{Sc_t} \rho_f^+ \partial_{y^+} X_i \right] + \partial_{y^+} j_{d,i,y}^+ = 0 \quad (8)$$

gives the mass-fraction profiles;

$$\partial_{y^+} u_{f,x}^+ = 1//(\mu^+ + \mu_t^+) \quad (9)$$

Table 1: Wall y^+ values at the centre cross-section, for selected coarse grids with uniform node spacing, for inlet velocities 0.2 and 0.4m/s.

No. of cells across channel	4	6	8	10
Inlet velocity				
0.2m/s	30	20	15	11
0.4m/s	49	36	25	20

gives the dimensionless axial fluid mixture velocity profile; and

$$\partial_{y^+}\left[K^+_{(0)}T^+ + K^+_{(1)}\partial_{y^+}T^+\right] = 0 \qquad (10)$$

gives the dimensionless temperature profile.

$$K^+_{(0)} \equiv \left(k^+_{f,c} + k^+_{f,t}\right)\left(\partial_{y^+}\ln c^+_P\right) - Pr_w\sum_{i=1}^{N}{}^+_{i,d,y}c^+_{P,i}, \qquad (11)$$

and

$$K^+_{(1)} \equiv k^+_f + k^+_{f,t} + k^+_{f,c} \qquad (12)$$

express the dimensionless groups in Eq. (10). For more details, refer to (Johnsen *et al.*, 2015).

Due to the assumed weak effect of thermophoresis (due to small temperature gradients) and the lack of good estimates of the thermophoretic diffusivity, only diffusiophoresis (concentration gradient diffusion) was considered in the current work. Furthermore, it was assumed that the model fluid could be treated as a dilute, ideal mixture. This reduces the Maxwell-Stefan diffusion model to the Fickian diffusion model. The mixture mass density and viscosity was modelled in accordance with (Pääkkönen *et al.*, 2015), while constant mixture thermal conductivity and specific heat capacity 0.6637W/m^2 of and 4182J/kgK, respectively, were used. The turbulent Schmidt number was set to 1. The Maxwell-Stefan binary diffusivity was tuned so that the area averaged deposition rate matched that of the experiments, for the $u_{f,x,in} = 0.2m/s$ data-point, and was kept constant for the other inlet velocities. This resulted in a Fickian diffusivity of $3.64 \cdot 10^{-5}m^2/s$.

CFD Models

CFD modelling was performed using the ANSYS FLUENT 16.2 CFD software. Turbulence is modelled with the standard $k - \varepsilon$ turbulence model. In the fine-mesh CFD model, the Enhanced Wall Treatment is employed to resolve the near wall region in the fine mesh model.

Temperature dependent fluid properties were implemented via user-defined functions (UDFs) in accordance with (Pääkkönen *et al.*, 2015). The fouling models were also implemented via UDFs and hooked into ANSYS Fluent via the adjust function hook. Due to the low deposition rates observed, it was expected that the mass transfer to the wall would have a very small effect on the bulk conditions in the coarse mesh. Thus, the fouling wall function was not utilized as a mass source, but was run on a frozen flow field.

Coarse-Mesh Velocity Wall Function

The fouling wall function was designed to work on grids where the grid cells residing on the wall are in the log-layer. The main reason for this is that its bulk boundary conditions were chosen to be valid for fully developed turbulent flow. In the current experimental set-up, however, due to the low Reynolds numbers, such a stringent requirement of the wall
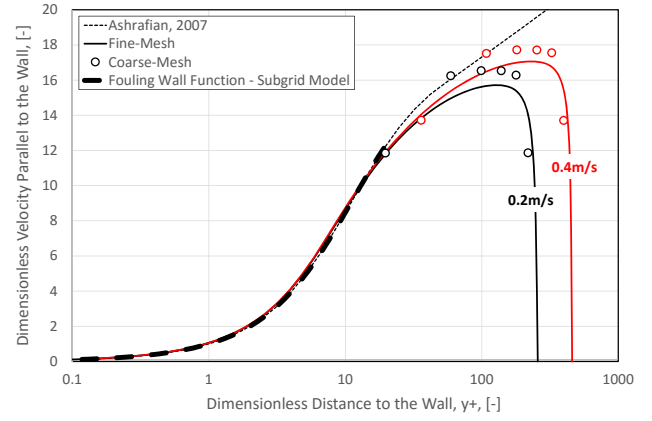
Figure 2: Comparison of dimensionless velocities as functions of dimensionless wall distance at the center cross-section (isothermal conditions), for the coarse- (circles) and fine-mesh (solid lines) CFD models, the fouling wall function subgrid model (dashed, black line), and theoretical velocity profile (Ashrafian and Johansen, 2007) (dotted, black line).

y^+ left us with very coarse meshes. In Table 1, the approximate wall y^+ value at the center cross-section (see Figure 1) is shown for various coarse meshes where the node spacing is constant across the channel.

In order to predict the wall shear stress and general velocity profile accurately, on the coarse mesh, the wall function proposed by Ashrafian and Johansen (2007), was employed;

$$u^+_{f,x}(y^+) = \begin{cases} 11.4\arctan\left(\frac{y^+}{11.4}\right), & y^+ \leq y^+_* \\ \frac{1}{\kappa}\ln\left(\frac{1+\kappa y^+}{1+\kappa y^+_*}\right) + u^+_{f,x}(y^+_*), & y^+ > y^+_* \end{cases}, \qquad (13)$$

with the dimensionless turbulent kinematic viscosity

$$\nu^+_t = \begin{cases} \left(\frac{y^+}{11.4}\right)^2 & y^+ \leq y^+_* \\ \kappa y^+ & y^+ > y^+_* \end{cases}, \qquad (14)$$

where dimensionless velocity is defined as $u^+_{f,x} = u_{f,x}/u_\tau$, dimensionless wall distance is defined as $y^+ = u_\tau y/\nu$, $y^+_* = 51.98$, and $\kappa = 0.42$ is the von Kármán constant.

A sensitivity study was done to investigate how the coarse meshes performed against the fine-mesh CFD model and the Ashrafian-Johansen wall function. It was determined that the mesh with 6 cells across the channel reproduced the fine-mesh velocity and temperature profiles quite well and at the same time gave an acceptable wall y^+ value. In Figure 2, it is shown how the fine-mesh and coarse-mesh CFD models perform against the profile published by Ashrafian and Johansen (2007) under isothermal conditions (no heating), in terms of dimensionless variables. The deviations at high y^+ values are due to the effect of the opposing channel wall and the relatively low Reynolds numbers investigated. For the coarse-mesh CFD model, the fouling wall function subgrid model is included for validation of the subgrid velocity profile. In Figure 3a, the coarse and fine-mesh axial velocity profiles at the center cross-section are compared, and in Figure 3b, the temperature profiles are compared. It can be seen that generally, the axial velocity was underpredicted, in the coarse-mesh CFD model, whereas the temperature was overpredicted.
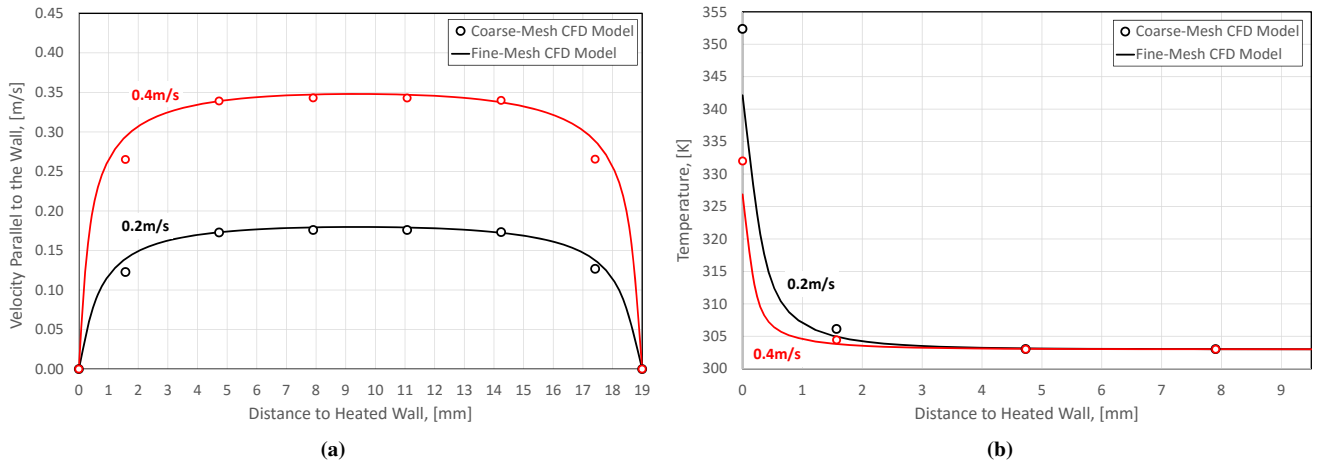
Figure 3: Comparison of parallel-to-wall flow velocity profiles (a) and temperature profiles (b) at the center duct cross-section ($x = 100mm$), for coarse and fine-mesh CFD models, for wall heat flux of $52.5kW/m^2$ and inlet velocities $0.2m/s$ and $0.4m/s$.

Boundary Conditions for the Fouling Wall Function

The fouling wall function requires boundary conditions for temperature and species mass-fractions at the wall as well as axial velocity, temperature and species mass-fractions in the bulk. The bulk values as well as the wall temperature are taken directly from the CFD model via the inbuilt macro library in ANSYS Fluent, and utilized as Dirichlet boundary conditions in the subgrid model. The species-specific mass-fraction boundary conditions at the wall, however, require special attention. First, the type of boundary condition depends on whether the species is depositing or not; second, they depend on which diffusive transport mechanisms are dominating close to the wall (Johnsen *et al.*, 2017).

E.g., consider the case where diffusion due to mass-fraction gradients (diffusiophoresis) is the sole transport mechanism close to the wall. For the non-depositing species, the mass-fraction gradient at the wall must be zero to ensure zero deposition flux, and we employ the Neuman BC for the ADE, at the wall. For the depositing species, however, we do not have a priori knowledge of the deposition flux, so we cannot use the mass-fraction gradient as a BC. We have to use the Dirichlet BC. That is, we need to specify the mass-fractions of the depositing species, at the wall.

The mass-fractions at the wall (interface mass-fractions) are consequences of the balance between transport through the turbulent boundary layer and the species integration into the crystal lattice. Therefore, it is a function of e.g. temperature, temperature gradient, composition, composition gradients, wall shear stress, crystal properties, etc. Thus, the interface mass-fraction is not just a fixed boundary condition, but is in fact part of the solution itself. If the kinetics of the surface reaction are known, it is possible to estimate the interface mass-fractions. Then, an iterative procedure can be employed to find the interface mass-fraction that ensures that the transport rate through the boundary layer and the integration rate into the crystal are identical (Johnsen *et al.*, 2017). Lacking accurate predictions of the surface reaction rates, the current wall function model employed interface concentrations obtained from the fine-mesh CFD model (see Figure 4). These concentrations are dependent on both wall temperature and inlet velocity (wall shear stress). By curve fitting the Logistic function,

$$X_{I,reg} = \frac{a}{1 + (T_w/b)^c} , \qquad (15)$$

Table 2: Curve fit polynomial coefficients for velocity dependence of interface mass-fractions (Eqs. 16-18).

	a	b	c
0	0.251654	342.436	409.600
1	1.28476	26.6133	−2179.69
2	−3.57731	−112.872	4968.05
3	3.41471		

to the fine-mesh CFD data, we obtained good representations of the interface mass-fractions for each inlet velocity case. The inlet velocity-dependent fitting parameters, a, b, and c, are shown in Figure 5, and could be accurately described in terms of 3rd and 2nd order polynomials;

$$a = a_0 + a_1 u_{f,x,in} + a_2 u_{f,x,in}^2 + a_3 u_{f,x,in}^3 , \qquad (16)$$

$$b = b_0 + b_1 u_{f,x,in} + b_2 u_{f,x,in}^2 , \qquad (17)$$

$$c = c_0 + c_1 u_{f,x,in} + c_2 u_{f,x,in}^2 . \qquad (18)$$

The coefficients are given in Table 2. Employing Eq. (15) with coefficients given by Eqs. 16-18, we got a good, general representation of the CFD-data (see black circles in Figure 5).

Figure 6 shows the temperature dependence of the calculated interface mass-fraction (Eq. (15)), for selected inlet velocity cases. It is seen that the interface mass-fraction drops from close to the bulk value to zero, at a certain threshold temperature, which appears to be dependent on the inlet velocity. In reality, this is a consequence of the complex interplay between mass deposition rate, interface mass-fraction, wall temperature, and wall shear stress. We will be content, however, to consider this as an inlet velocity dependent feature. At temperatures below the threshold, the deposition regime is interface controlled, whereas at higher temperatures it is diffusion controlled. Pääkkönen *et al.* (2012) concluded that the fouling regime was interface controlled, in these experiments, since the over-all deposition rate is not increasing for increasing flow-velocities, as would be expected for a mass transfer controlled fouling regime. However, various segments of the heated wall may be in different fouling regimes depending on the local flow conditions and wall temperature, as indicated in Figure 7. In general, the higher the difference between the bulk and interface mass-fractions, the higher
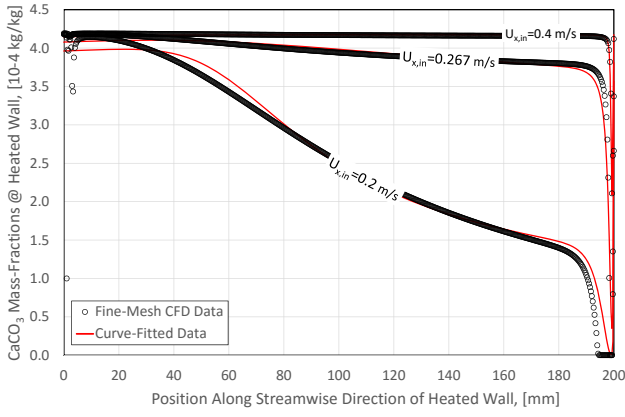
Figure 4: Comparison of fine-mesh CFD (black circles) and best-fit (red lines) $CaCO_3$ mass-fractions at the wall plotted against the axial position along the heated wall, for selected inlet velocities.
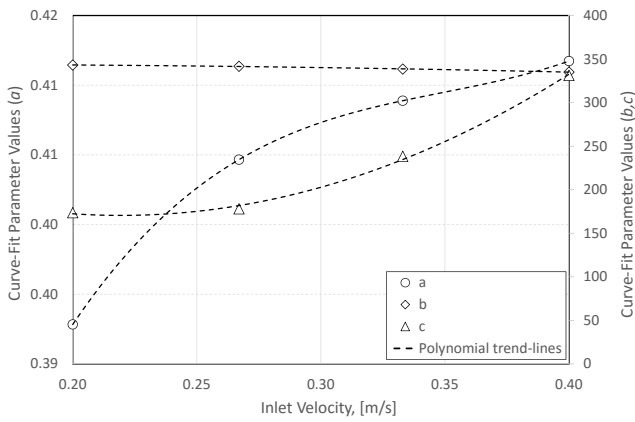

Figure 5: Curve-fit parameters a, b, and c (see Eq. (15)) plotted as functions of inlet velocity, along with best-fit polynomial trend-lines (see Eqs. 16-18 and Table 2).
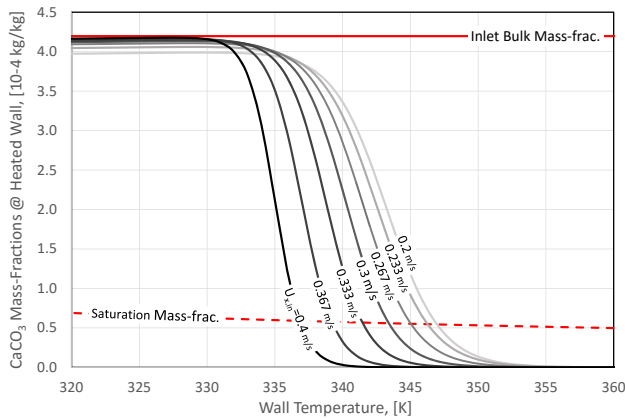

Figure 6: Comparison of temperature dependency of $CaCO_3$ bulk (red line), saturation (dashed red line), and interface (calculated for various inlet velocities, from Eq. (15): black= $0.4 m/s$, light gray= $0.2 m/s$) mass-fractions, at the wall.

the deposition rate (mind that at interface mass-fractions below the metastable equilibrium mass-fraction, fouling might not take place at all). Thus, the deposition rate at locations with wall temperatures above the threshold can be expected to dominate. Since the coarse-mesh CFD model is
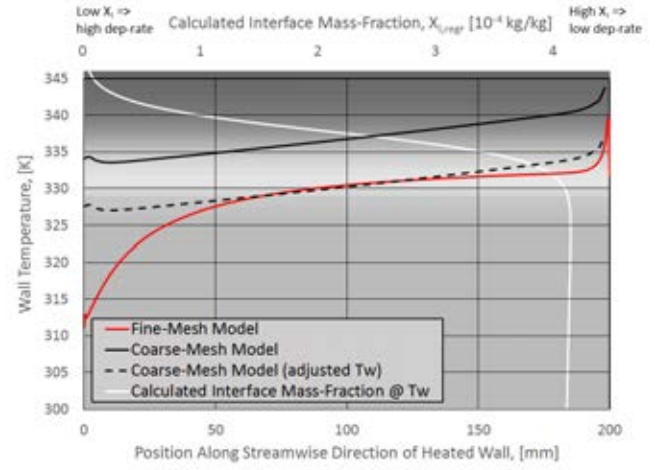

Figure 7: Wall temperature vs. position along the heated wall, for the $u_{f,x,in} = 0.333 m/s$ case, for the fine-mesh model (red), coarse-mesh model (solid black), and adjusted coarse-mesh wall-temperature ($-6.5K$) (dashed black). The relationship between the wall temperature and the interface mass-fraction is shown by the white curve. The contour plot in the background corresponds to the interface mass-fraction values at given wall temperatures (dark gray corresponds to low X_I, and light gray corresponds to high X_I) and links the modelled, local wall temperatures with an expected local interface mass-fraction.

prone to overpredict the wall temperature, as was discussed above (see Figure 3b), there is a risk that the interface mass-fraction is severely underpredicted if the true wall temperature is lower than, but close to the threshold temperature. To reduce the risk of overprediction of deposition rates, a fixed $6.5K$ was subtracted from the wall temperature when calculating the interface mass-fraction from Eq. (15). Figure 7 shows that a greater part of the overpredicted wall temperature curve (solid black) is in the low interface mass-fraction region (dark gray area) than the fine-mesh model wall temperature curve (red). Hence, a greater part of the wall will have low interface mass-fraction in the coarse-mesh model than in the fine-mesh model. The corrected wall temperature curve (dashed black), however, is more similar to the fine-mesh model temperature curve. Furthermore, interface mass-fractions below the saturation mass-fraction indicate that the fluid is undersaturated at the crystal surface. Physically this means that deposition is unfavorable with respect to minimizing the Gibbs free energy, thus no deposition will take place (Johnsen *et al.*, 2017). Therefore, the Dirichlet boundary condition for the $CaCO_3$ was set to

$$X_{I,CaCO_3} = \max\left(X_{I,reg}, X_{Sat}\right) . \qquad (19)$$

RESULTS AND DISCUSSION

The ambition in the current work was to demonstrate the applicability of a previously developed fouling wall function framework (Johnsen *et al.*, 2015), in practice. To approach this objective, its implementation, as a user-defined function in ANSYS Fluent 16.2, was employed to demonstrate how it performs against a more traditional two-step fouling modelling approach (Pääkkönen *et al.*, 2016), in the context of a well-controlled laboratory experiment (Pääkkönen *et al.*, 2012).

The main motivation for developing the fouling wall function was to eliminate the need to resolve the turbulent boundary layer and enable efficient fouling modelling in industry scale
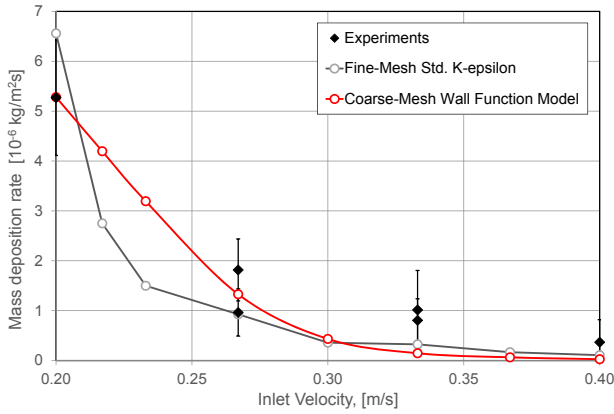
Figure 8: Comparison of the area averaged mass deposition rates from the fine-mesh two-step model and the coarse-mesh fouling wall function model with the experimental data.
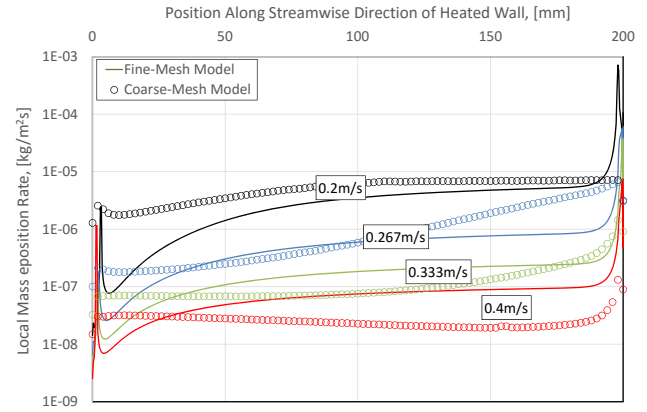

Figure 9: Comparison of the local mass deposition rates calculated by the fine-mesh two-step model (lines) and the coarse-mesh fouling wall function model (circles), at selected inlet velocities.

CFD simulations. Hence, the modelling framework relies on relatively high wall y^+ values in the CFD cells residing at the wall. This proved to be challenging in the employment of the above cited experimental and simulation data, for comparison. Due to the low Reynolds numbers encountered in the data from Pääkkönen et al., it was necessary to confide in a very coarse CFD mesh as basis for the fouling wall function modelling (see Figure 1).

The mass deposition rates predicted by the fouling wall function are depending directly on the wall function boundary conditions;

- wall mass-fractions for the depositing species,
- bulk and wall temperatures,
- bulk velocity parallel to the wall,

where *bulk* refers to the center of the CFD grid cells residing at the wall. Thus, accurate prediction of the deposition rates rely heavily on the accurate CFD modelling of these quantities.

By utilizing the wall function published by Ashrafian and Johansen (2007), we managed to reproduce the fine-mesh CFD model velocity and temperature profiles fairly well, qualitatively. However, the quantitative discrepancy turned out to be the major source of error in the fouling wall function modelling results. In Figure 2, it can be seen how the dimensionless velocity profiles are comparable in the absence of heating, and in Figure 3 it can be seen how dimensional velocity and temperature profiles are comparable under constant heating of $52.5 kW/m^2$. The effect on the velocity profiles, by turning on/off heating was minimal.

Since thermophoresis was neglected in the current work, the role of the temperature was to provide the temperature dependent fluid properties (mass density, viscosity, and saturation mass-fraction), and interface mass-fraction for the depositing species. Although the inaccurate prediction of any of these will affect the predicted mass deposition rate to some extent, it seemed that the effect of the inaccurate prediction of the interface mass-fraction was the most severe. As was indicated in figures 6 and 7, even modest errors in the local wall temperature could result in a severely miss-represented interface mass-fraction. Since the mass deposition rate is expected to scale approximately linearly with the difference between the bulk and interface mass-fractions, the mass deposition rate can be off by an order of magnitude by just a slight overprediction of the wall temperature, as seen in Figure 6. To avoid underpredicting the interface mass-fraction due to overprediction of the wall temperature, the temperature was

subtracted a fixed $6.5K$ when calculating the interface mass-fractions (see Figure 7).

Figure 8 presents a comparison between the experimental data, the fine-mesh two-step fouling model data, and the data obtained from the coarse-mesh fouling wall function model. In the absence of reliable measurements/calculations of the diffusivity, it was treated as a calibration parameter, for the fouling wall function. The fouling wall function data were thus obtained with a tuned diffusivity of $3.64 \cdot 10^{-5} m^2/s$, reproducing the $u_{f,x,in} = 0.2 m/s$ experimental data point. The same, constant diffusivity was used in all grid cells along the wall, for all the inlet velocity cases. Despite the issues with predicting the required boundary conditions for the fouling wall function model accurately, the modelling results compared very well with the results from the fine-mesh two-step fouling modelling and the experimental data, in terms of the area averaged mass deposition rate.

In Figure 9, the local deposition rates are compared for the fine-mesh two-step model and the coarse-mesh fouling wall function model. It can be seen that even if the area-averaged values compared well, the local values differs significantly. The mismatch seems primarily to be due to

- inaccurate prediction of interface mass-fraction;
- inaccurate prediction of wall temperature in the coarse mesh;
- inaccurate prediction of bulk velocity in the coarse mesh.

The most crucial improvement to the fouling wall function model would be to get accurate interface mass-fractions. An in-depth study of these effects are left to future investigations. In the meantime, we are content to summarize that the fouling wall function approach performed very well in a scenario, slightly outside the design specifications of the modelling framework, with respect to the Reynolds number. The model fluid used in the current paper is a coarse simplification of the actual fluid employed in the cited experiments. The real fluid was a salt-water solution involving a multitude of chemically reacting ions and molecules. This is reflected by the fact that the content of dissolved $CaCO_3$ in the model fluid, is much higher than the saturation concentration. Thus, the modelled $CaCO_3$ may be seen as a pseudo-component representing e.g. the true $CaCO_3$ fraction in addition to Ca^{2+}, CO_3^{2-} and possibly other species. In the present case, at relatively low concentrations, this simplification seems to be justified in both modelling approaches

employed. However, this may be part of the explanation of the local difference between deposition rates resulting from the two modelling methods.

The present demonstration case indicates that in industry-scale applications, where very fine meshes are infeasible, the wall function approach may provide a means to do physically detailed simulations of complex fluids, in complex geometries, at reasonable computational cost. In particular, if it can be assumed that the deposition rates are so small that they do not affect the flow field significantly, the savings in computational cost will be great. Then, the fouling wall function can be run on a frozen flow-field, and sensitivity studies or optimization studies on e.g. diffusivities, wall surface properties, etc., that does not affect the macro scale flow-fields can be performed without the need to update the frozen flow-field. Establishing the frozen flow-field on the coarse mesh, without the fouling wall function activated is very efficient due to the low number of computational cells needed. Then, running multiple fouling scenarios can be done on that flow-field just by changing input parameters to the fouling wall function and running one single CFD iteration, for each fouling scenario, with the fouling wall function activated.

CONCLUSION

Two different CFD modelling approaches were compared with experimental data on mass deposition rates in an experimental heat exchanger set-up. The two CFD strategies resolved the fine length-scales determining the mass transfer through the turbulent boundary layer, in two different ways: 1) the refinement was done in the 2D CFD mesh, resulting in a relatively high number of grid cells and a wall y^+ of ca. 0.08; and 2) the refinement was taken into account in a wall function utilizing a 1-dimensional subgrid, allowing for a coarse CFD mesh with wall y^+ of about 30. The fine-mesh CFD model utilized a traditional two-step modelling approach for the mass deposition modelling, complemented with the fluid residence-time at the wall, whereas the coarse-mesh CFD model wall function solved the coupled Advection-Diffusion, momentum and energy equations on a local subgrid to estimate the mass deposition rates.

The coarse-mesh model performed very well compared to the fine-mesh model and experimental data, with respect to area average deposition rates. Significant mismatch was observed, however, in the local deposition rates. The lacking accuracy in the coarse-mesh model was mainly due to the challenges in predicting interface mass-fractions, wall temperatures and bulk velocities, on the very coarse mesh.

The over-all good performance of the coarse-mesh model gives strong support to the idea that the wall function approach may provide a means to do physically detailed simulations of complex fluids, in complex, industry-scale geometries, at a reasonable computational cost.

ACKNOWLEDGEMENTS

REFERENCES

ASHRAFIAN, A. and JOHANSEN, S.T. (2007). "Wall boundary conditions for rough walls". *Progress in Computational Fluid Dynamics*, **7(2-4)**, 230–236.

AUGUSTIN, W. and BOHNET, M. (1995). "Influence of the ratio of free hydrogen ions on crystallization fouling". *Chemical Engineering and Processing: Process Intensification*, **34(2)**, 79–85.

BANSAL, B., CHEN, X.D. and MÜLLER-STEINHAGEN, H. (2008). "Analysis of 'classical' deposition rate law for crystallisation fouling". *Chem. Eng. Process.: Process Intensification*, **47**, 1201–1210.

BRAHIM, F., AUGUSTIN, W. and BOHNET, M. (2003). "Numerical simulation of the fouling process". *International Journal of Thermal Sciences*, **42(3)**, 323 – 334.

HELALIZADEHA, A., MÜLLER-STEINHAGEN, H. and JAMIALAHMADIA, M. (2005). "Mathematical modelling ofmix ed salt precipitation during convective heat transfer and sub-cooled flowboiling". *Chemical Engineering Science*.

JOHANSEN, S.T. (1991). "The deposition of particles on vertical walls". *International Journal of Multiphase Flow*, **17(3)**, 355–376.

JOHNSEN, S.G. and JOHANSEN, S.T. (2009). "Deposition modelling from multi-phase dispersed flow - a boundary layer wall function approach". *Heat Exchanger Fouling and Cleaning VIII - 2009*.

JOHNSEN, S.G., ÅBERG, M. and JOHANSEN, S.T. (2010). "Implementation and demonstration of a boundary condition wall function for industrial scale particulate fouling cfd modeling". *ICMF 2010 7th International Conference on Multiphase Flow, Tampa, Florida, USA*.

JOHNSEN, S.G., JOHANSEN, S.T. and WITTGENS, B. (2015). "A wall-function approach for direct precipitation/crystallization fouling in cfd modelling". *Heat Exchanger Fouling and Cleaning XI - 2015*.

JOHNSEN, S.G., JOHANSEN, S.T. and WITTGENS, B. (2016). "Implementation and demonstration of a boundary condition wall function for direct precipitation fouling cfd modelling". *ICMF 2016 9th International Conference on Multiphase Flow, Firenze, Italy*.

JOHNSEN, S.G., PÄÄKKÖNEN, T.M., ANDERSSON, S., JOHANSEN, S.T. and WITTGENS, B. (2017). "On the wall boundary conditions for species-specific mass conservation equations in mathematical modelling of direct precipitation fouling from supersaturated, multi-component fluid mixtures". *arXiv:1703.01448 [physics.flu-dyn]*.

KLEIJN, C.R., VAN DER MEER, T.H. and HOOGENDOORN, C.J. (1989). "A mathematical model for lpcvd in a single wafer reactor". *Journal of The Electrochemical Society*, **136(11)**, 3423–3433.

KRISHNAN, A., NING, Z. and PRZEKWAS, A. (1994). "A computational model for chemical vapor deposition processes in industrial reactors". *4th InterSociety Conference on Thermal Phenomena in Electronic Systems (I-THERM)*, 222–236.

MÜLLER-STEINHAGEN, H. (2011). "Heat transfer fouling: 50 years after the kern and seaton model". *Heat Transfer Engineering*, **32(1)**, 1–13.

MULLIN, J.W. (2001). *Crystallization*. Butterworth-Heinemann.

MWABA, M.G., GOLRIZ, M.R. and GU, J. (2006). "A semi-empirical correlation for crystallization fouling on heat exchange surfaces". *Applied Thermal Engineering*, **26(4)**, 440–447.

PÄÄKKÖNEN, T.M., RIIHIMÄKI, M., SIMONSON, C.J., MUURINEN, E. and KEISKI, R.L. (2012). "Crystallization fouling of $CaCO_3$ - analysis of experimental thermal

resistance and its uncertainty". *International Journal of Heat and Mass Transfer*, **55(23-24)**, 6927 – 6937.

PÄÄKKÖNEN, T.M., RIIHIMÄKI, M., SIMONSON, C.J., MUURINEN, E. and KEISKI, R.L. (2015). "Modeling *CaCO$_3$* crystallization fouling on a heat exchanger surface - definition of fouling layer properties and model parameters". *International Journal of Heat and Mass Transfer*, **83**, 84–98.

PÄÄKKÖNEN, T.M., OJANIEMI, U., PÄTTIKANGAS, T., MANNINEN, M., MUURINEN, E., KEISKI, R.L. and SIMONSON, C.J. (2016). "CFD modelling of *CaCO$_3$* crystallization fouling on heat transfer surfaces". *International Journal of Heat and Mass Transfer*, **97**, 618 – 630.

WITTGENS, B. (2013). "Score - staged combustion for energy recovery in ferroalloy industry". http://www.sintef.no/en/projects/score-staged-combustion-for-energy-recovery-in-fer/.